MOLECULAR DYNAMICS SIMULATION OF THIN FILMS DEFORMATION

A.V. Bolesta[1,a], V.M. Fomin [1,b]

[1] Khristianovich Institute of Theoretical and Applied Mechanics, Institutskaya str., 4/1, Novosibirsk, 630090, Russia

[a] bolesta@itam.nsc.ru, [b] fomin@itam.nsc.ru

Keywords: molecular dynamics; thin films; deformation; indentation; uniaxial tension; cycled loading; interface; chessboard structure.

Abstract. We report on the results of a molecular dynamics study of the behavior of thin copper films under external loading. Loadings of two types were examined: indentation and uniaxial deformation. For the structural state of the films, either a single crystal or a finely dispersed polycrystal was assumed. The state of the free surface of the film and the choice for the type of indenter in modeling the indentation tests were varied as well.

Introduction

The use of thin films in integrated circuits and sensors raises important points concerning the mechanical properties of solids and the interaction between them at micro-scale level. Because of the small thickness of the films, the volume fraction of atoms located near the free surfaces and interfaces between materials becomes essential, making the contribution of those atoms to the behavior of the composite material also significant. Because of the extremely small spatial scales defining the thickness of near-surface and near-interface layers, continual models fail to give an adequate description to the whole spectrum of observed physical phenomena [1-6]. In modeling the mechanical behavior of such systems the latter necessitates explicitly taking the discrete structure of the medium into account, which can be made using the molecular-dynamic approach. In the present paper, different types of loading were considered: indentation and uniaxial tension. Two structural states of the films of interest were considered, one state being a defect-free single crystal and the other state, a polycrystal with grain size of several nanometers. Primary attention was paid to revealing and correlating the features observed in the loading curves with the processes proceeding on the atomic level.

Molecular dynamics modeling

The interaction between the copper and aluminum atoms was described using an inter-atomic potential calculated within the framework of the embedded atom method (EAM) [7,8]. The multi-particle EAM has showed itself to good advantage in modeling deformed metal clusters and heterostructures [9-11]. The motion trajectories were calculated with the help of the LAMMPS parallel molecular-dynamic software package [12]. The equations of motion of atoms were integrated using the velocity Verlet algorithm. For identification of lattice defects in the crystal, the centrosymmetry parameter P has been used [13]. The value of P is known to be close to zero for atoms whose local coordination is such as that in the fcc lattice, and it increases markedly when a stacking fault appears in the lattice, and also for surface atoms. The quasi-static uniaxial stretching and compression of the composition were modeled using periodic scaling of the calculation-cell size in prescribed direction with consequent relaxation of the system between the times of scaling. Along this direction, periodic boundary conditions were applied to the system. The rate of deformation of the calculation-cell was $3 \cdot 10^8 \mathrm{s}$. The indenter action was modeled by pressing into the material a

hemisphere that repulsed all atoms around it. Thus, the indenter was assumed rigid and structureless. Although, normally, in nanoindentation tests indenters shaped as pyramids are used, indenters always have a finite radius of tip curvature, which normally amounts to several ten nanometers. That is why on the spatial scale treated with the molecular-dynamic method the indenter can be considered spherical. The indenter velocity was assumed to be 10 m/s. Since this velocity was two orders lower than the speed of sound in copper, the deformation of examined film was quasi-static. Nonetheless, it should be noted that at temporal scales typical for molecular dynamics calculations diffusion processes never manifest themselves. That is why the calculated data have limited application in consideration of the indentation problem at high temperatures. The indenter curvature radius R was assumed to range from 1 to 10 nm. With the aim to review the effect of the spherical shape of the indenter on modeled data, we consider the problem on indentation and scratching of a copper film with a sharp diamond indenter. In modeling the perfectly rigid substrate onto which the film was applied, the lower atomic layer was assumed fixed, so that it always remained stationary.

Uniaxial tension of thin copper film

The results of this section have been published earlier [14]. A copper film was modeled with a parallelepiped, sized $28.9\times28.9\times14.4$ nm, which comprised about one million atoms, with periodic boundary conditions applied in two surface-parallel directions. The crystallographic orientation of the crystallite was such that the directions [100], [010] and [001] were coincident with coordinate axes. Since the effect due to clamps neglected, the material experiences rather a high (about 10%) limit of elasticity in stretched monocrystalline copper films with ideal free surfaces (Fig. 1). The nucleation of an initial stacking fault whose subsequent development causes plastic deformation in the film is hindered due to a high potential barrier which the atomic system has to overcome. Next, after the first staking fault has nucleated, the initial symmetry of the system becomes violated, and the stress in the sample decreases three-fold.

The surfaces of real materials are always rough at different scales. In this connection, it would be of interest to analyze the effect of surface roughness on the loading diagram in indentation of a thin film whose surface is not perfectly smooth. To this end, we modeled the indentation of a smooth monocrystalline film with rough free surface. Again, the copper crystallite was chosen to be shaped as a parallelepiped, with periodical boundary conditions applied in two surface-parallel directions. The crystallographic orientation of the crystallite was chosen such that the directions [100], [010] and [001] were coincident with coordinate axes. In modeling roughness, the Fourier filtration method was employed [15, 16], which was used to define the free-surface profile of the crystallite. After letting the formed atomic system relax at temperature 300 K to equilibrium state, a thin film was formed, whose surface was self-affine over the length scale from the lattice-constant value $a=0.36$ nm to the calculation cell size $L_{\max}=36$ nm, with fractal dimension $D_f=2.3$ [16]. Addition of roughness to one of the free surfaces results in that, in the rough film, the transition to plastic deformation occurs much earlier, already at $\varepsilon=0.05$ (Fig. 1). The latter points to a considerable lowering of the potential barrier for the formation of a stacking fault right near surface cavity. After the limit of elasticity is overcome, plastic deformation of the film proceeds as a result of the development of a system of lattice defects.

Subsequent lowering of the potential barrier for the passage to plastic-deformation regime was observed for deformation of a polycrystalline film with grain size about 2 nm. The formation of a polycrystalline film was modeled by simulating the quenching of the material from the melted state at temperature 1500 K to the solid state at temperature 300 K (rate of quenching $1.2\cdot10^{13}$ K/c) followed by relaxation of the atomic system at temperature 300 K lasting for a time interval 40 ns. The relaxation was modeled using the Nose-Hoover thermostat algorithm [17]. An analysis of the radial distribution function has showed that, during the relaxation, long-range order has established

in the mutual location of the atoms (Fig. 2a). Fig. 2b shows a cross-sectional view of the polycrystalline film formed as described above. The structure of the crystal lattice comprises many point and planar defects, the typical grain size being 2 nm. In the calculations, the thickness of the copper film was 9 nm, and the transverse sizes were 18 nm. In both transverse directions periodic boundary conditions were applied. The elastic part of $\sigma - \varepsilon$ diagram ($\varepsilon < 1.5\%$) shows almost no differences from the straight lines obtained for the monocrystalline film (Fig. 1), the latter being the consequence of the good isotropy of the elastic properties of copper. The maximal stress of 1.4 GPa is attained here already at 2-% strain. This value is in good agreement with experiments for high speed deformation of nanostructured copper [18].

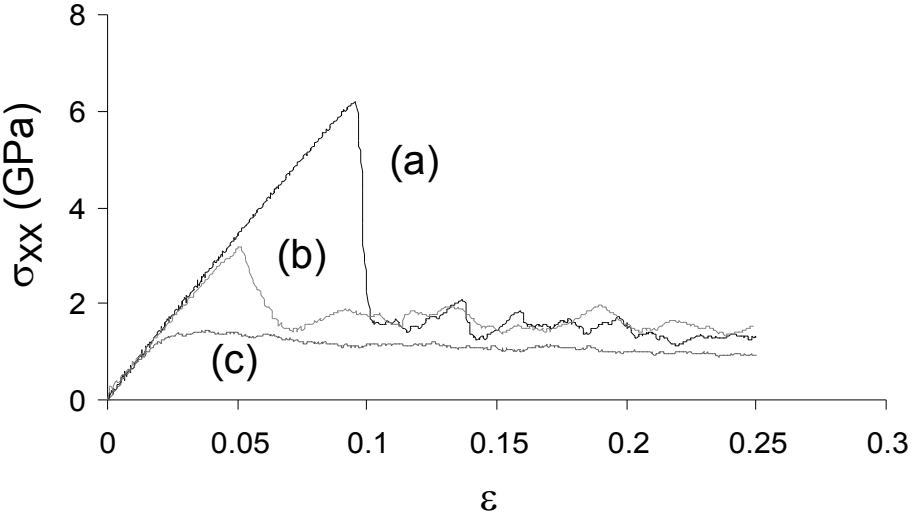

Fig.1 The strain-stress diagrams of single crystal film with ideal free surfaces (*a*), crystallite with one free surface having 2.5-nm roughness and fractal dimension $D_f = 2.3$ (*b*), and polycrystalline film (*c*).

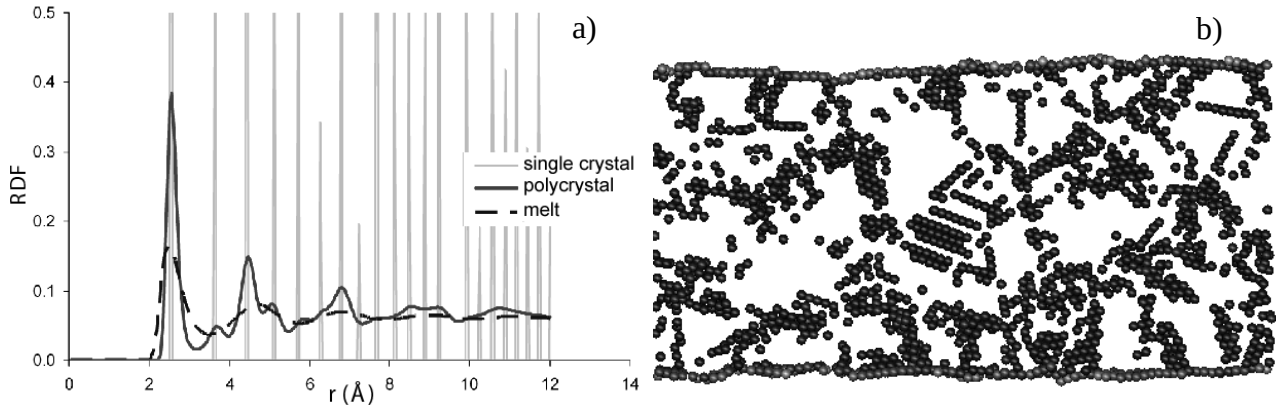

Fig.2 Radial distribution function of monocrystalline, polycrystalline, and melted copper (a) and cross-sectional view of the polycrystalline film (b). Atoms with local coordination differing from that in the fcc lattice are only shown.

Indentation of thin copper film with spherical indenter

The results of this section have been published earlier [19]. Fig. 3a shows the curve of the force of indenter interaction with substrate F_z versus the indenter penetration h. At the initial stage of penetration ($h < 5$Å), the substrate material deforms elastically. This portion of the loading curve obeys the Hertz contact theory. Over the elastic portion, the unloading curve closely follows the

loading curve. At larger penetrations ($h > 5$Å), the material displays an elasto-plastic response with a hysteresis observed in the loading-unloading curve. The indenter action results in the formation of a crater on the copper surface, with some portion of the material forced to the surface around the crater (Fig. 3b). The plastic deformation of the substrate is accompanied by nucleation of lattice defects in the bulk of material under the indenter, and the displaced atoms get incorporated into additional atomic layers around the crater. On the transition to the elasto-plastic deformation regime, lattice defects start nucleating in the bulk of the thin film under the indenter, and then these defects propagate deeper into the material bulk.

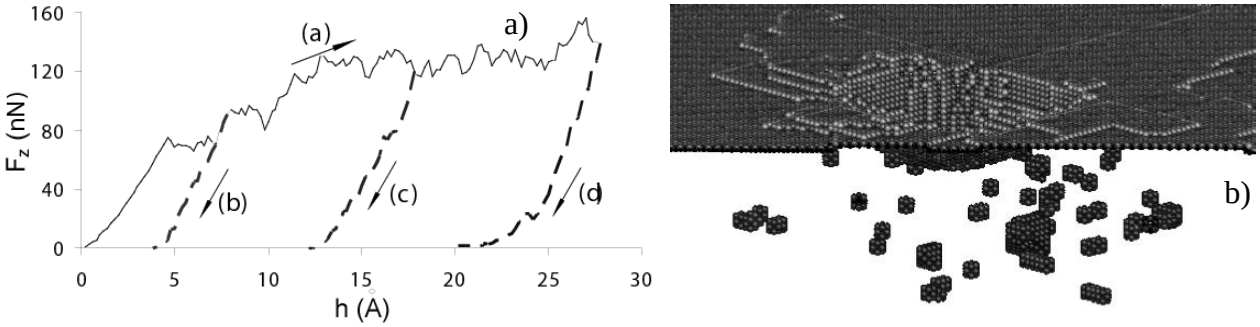

Fig.3 Applied load versus the depth of indenter penetration into the monocrystalline copper film on a rigid base (a). Indenter radius - 2 nm. Film thickness - 14.4 nm. Loading and unloading curves (*a* and *b*-*d*, respectively) are shown. And the copper film after the loading-unloading cycle (b). Atoms with local coordination differing from that in the fcc lattice are only shown.

An important experimentally measured characteristic of the materials is hardness. For a spherical indenter, the hardness is normally calculated using the standard Brinell formula

$$BHN = \frac{F_z^{\max}}{2\pi R\left(R - \sqrt{R^2 - R_i^2}\right)} \qquad (1)$$

where R_i is the indenter imprint radius. The radius R_i was calculated using the approximation of the indenter imprint edge after the removal of the load with a circle (Fig. 4a). An estimate of the hardness of single crystal copper by Eq. (1) yields rather high hardness values of 6–15 GPa (Fig. 4b). In view of this, with the atomic nature of the imprint taken in consideration, the determination accuracy of R_i was rather low. For instance, for an indenter with 1 nm radius this accuracy could be estimated as 20%, whereas for an indenter with 5 nm, as 5%. Two major tendencies can be revealed in the behavior of data in Fig. 4b. First, a decrease in the indenter radius leads to an increased estimated hardness. Thus, the maximal hardness values are observed when a film is indented with a ball of radius 1 nm, the latter radius being as small as several interatomic distances. Second, with increase in indenter penetration the film hardness decreases because of the accumulation of stacking faults in the volume of the copper as the indenter penetrates deeper into the film.

The calculation of the Brinell hardness for the polycrystalline film (Fig. 4b) has showed that, unlike the single crystal film, here the dependences on the indenter radius and penetration are manifested weakly. The hardness values, 5-6 GPa, now lie much closer to the experimental value of 3.5 GPa obtained in microidentation tests of polycrystalline copper samples at temperature 200 K [6]. Note that it is the hardness on Vickers scale that was measured in the cited experiments, and films with larger grain size, 11 nm, were investigated. Nonetheless, substantial convergence of the spatial

scales recently achieved in advanced nanoindentation tests of ultra-dispersed materials and in molecular-dynamic simulations seems attractive.

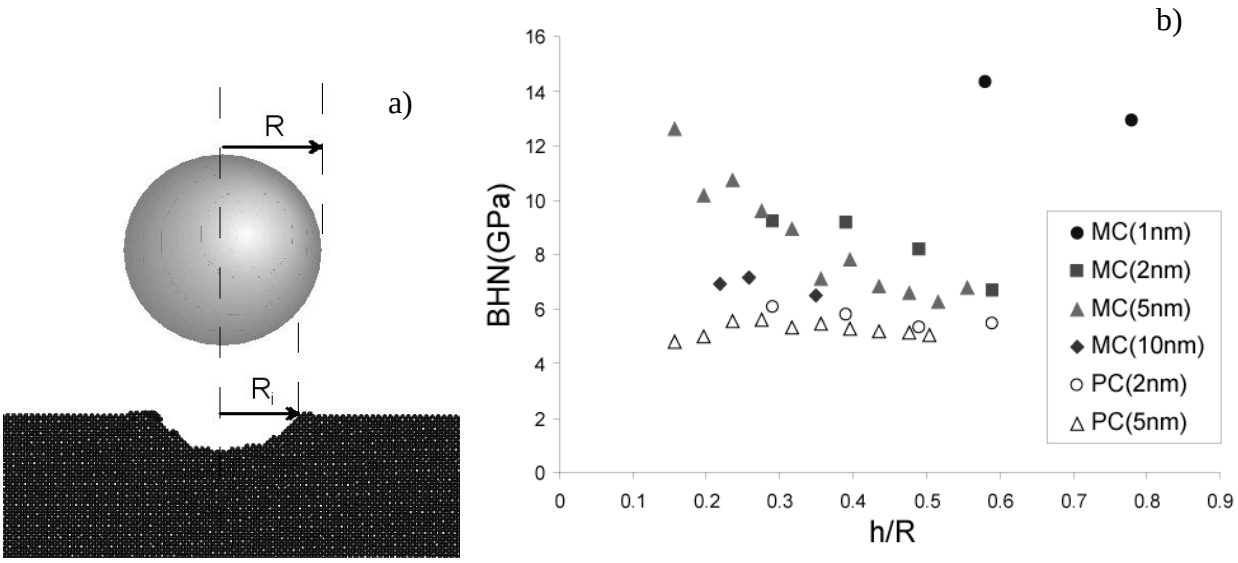

Fig.4 Determination of the imprint radius R_i in indentation of a film with a spherical indenter of radius R (a) and estimated Brinnel hardness for monocrystalline (MC) and polycrystalline (PC) copper film as a function of the indenter penetration normalized by the indenter radius R (b). Data for R = 1, 2, 5, and 10 nm are shown.

Indentation and scratching of thin monocrystalline copper film with a diamond indenter

With the aim to examine the effect of indenter shape on the results of modeling of indentation of a thin copper film, we performed a molecular dynamics simulation of the interaction of a diamond indenter with a monocrystalline copper film. The indenter was a trihedral pyramid formed by carbon atoms located at diamond-lattice sites, this being an analog to Berkovich pyramid (Fig. 5a). The interaction between carbon atoms was modeled using an inter-atomic potential calculated within the framework of a modified embedded-atom method [20]. The interaction between copper and carbon atoms was represented with the Morse potential; this, in contrast to the case of a rigid spherical indenter, brought about an adhesion-induced component into the force of indenter interaction with the film surface. The copper substrate was modeled as a parallelepiped, sized $36.2\times14.5\times7$ nm, with periodic boundary conditions applied in two surface-parallel directions. The crystallographic orientation of the crystallite was chosen such that the directions [100], [010] and [001] were coincident with coordinate axes. The lower atomic layer was stationary, and the substrate was taken to be large enough for the effect due to finite calculation-cell sizes to be excluded.

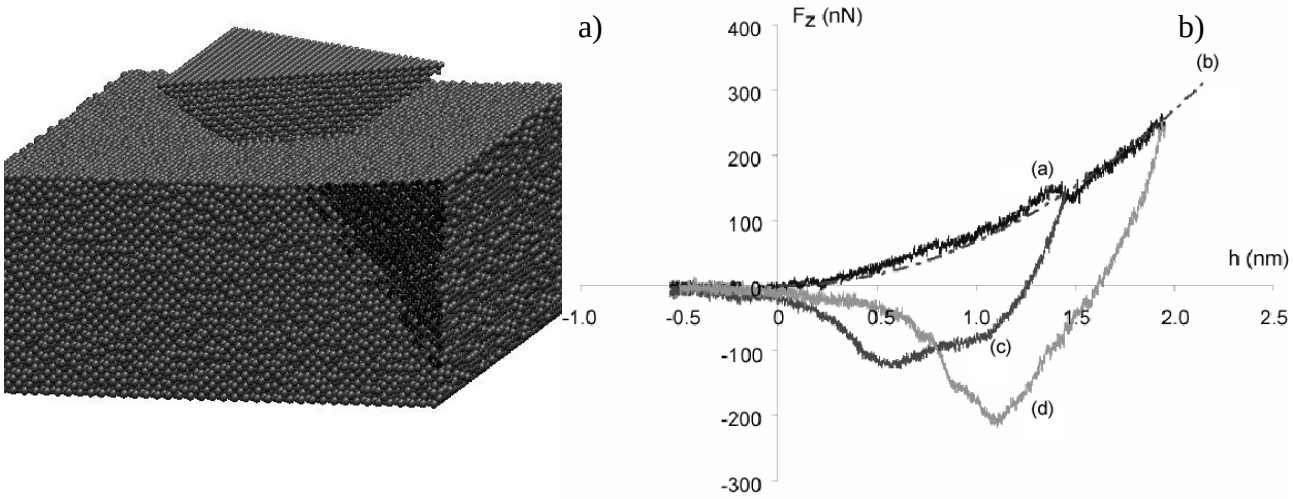

Fig.5 The copper film indented with a diamond indenter (a) and the loading diagram of a copper film indented with a diamond indenter: *a* – loading curve, *b* – fit of the loading curve with Eq. (2), *c* and *d* – unloading curves (b).

Like in the case of a spherical indenter, the indentation process was modeled as penetration, at fixed velocity, of a diamond pyramid into the film with subsequent withdrawal of the indenter out of the material. Unlike in the case of a spherical indenter, the calculated loading curve (curve *a* in Fig. 5b) from the very beginning ascends according to the law of h^2. The latter is related with the fact that the indenter was sharp, the curvature radius of its tip being the order of lattice constant. That is why the film from the very beginning underwent deformation in plastic regime. For comparison, Fig. 5b shows the curve

$$F_H = HS = 4.5Hh^2. \qquad (2)$$

(curve *b*), where S is the contact area of the pyramidal indenter with the film, and $H = 15\,\text{GPa}$. Note that the hardness level of 15 GPa is quite comparable with the value that was observed in indentation of the film with the sharp spherical indenter (see Fig. 4). Also, the fact deserves mention that, here, the area S in Eq. (2) is the contact area for the material that can be elastically restored on unloading, which process proceeds with participation of the adhesive interaction of the indenter with the film (in unloading curves *c* and *d*, Fig. 5b, curve portions with negative values of F_z are observed). As a result, the imprints after unloading turn out to be distorted. The decrease in the contact area due to unloading-induced restoration is partially compensated by the sticking of the film material to the indenter mediated by attracting forces. As a result, the estimate of the imprint sizes obtained after unloading turns out to be close to the value $S = 4.5h^2$ used in Eq. (2). Thus, like in the case of a small-radius spherical rigid indenter, the use of a perfectly sharp pyramidal diamond indenter results in obtaining a monocrystalline-copper hardness value 15 GPa predicted by calculations in the previous section

The accuracy in evaluation of the imprint size can be substantially improved using scratching of the material surface with a Berkovich pyramid. Fig. 6a shows such an imprint as revealed through an analysis of molecular dynamics data. As the pyramid moves along the surface, some portion of the material gets forced to imprint periphery; this can be expected to facilitate the measurement of the imprint size and to improve the accuracy in such measurements. Here, the indentation was made to 1.5-nm depth in a time interval of 200 ps. Then, the pyramid was imparted with a constant velocity

10 m/s directed along the film surface. During the next 400 ps the indenter motion was stabilized at a level of $F_z = 170\,\text{nN}$ and $F_x = 200\,\text{nN}$ (Fig. 6b), the latter values referring to rather a high value of the adhesion-force-induced friction coefficient, 0.85.

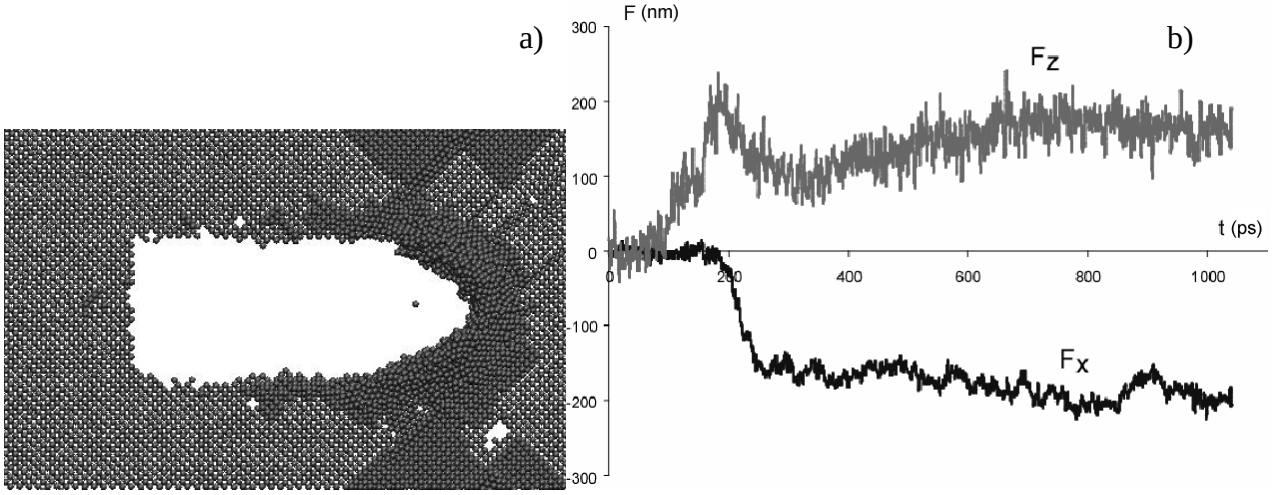

Fig.6 An imprint obtained by scratching the monocrystalline copper film with a diamond indenter (a) and indentation force F_z and friction force F_x versus time for the copper film scratched with a diamond indenter (b).

Thus, using a molecular dynamics model for the interaction of a diamond indenter with the surface, we showed that taking the actual structure of diamond indenter into account does not modify substantially the loading picture, the only exception being the emergence of a curve portion with a negative interaction force, this portion being a result of the adhesive interaction between copper and carbon atoms. The estimated hardness complies with the data, obtained in indentation of copper surface with the sharpest spherical indenter.

Summary

Molecular-dynamic modeling of quasi-static deformation of a thin copper film was performed. For uniaxial tension it is shown that the state of the free surface has a profound influence on the elastic limit of monocrystalline copper films: surface roughness acts to decrease the elastic limit two-fold, from 10% to 5%. On the other hand, uniaxial deformation of a polycrystalline finely dispersed copper film with 2-nm typical grain size shows an even larger reduction of the elasticity limit, down to 1.5%. It was shown that in indentation of monocrystalline copper films with spherical indenters with tip radius smaller than 10 nm the estimated hardness of such films with atomically smooth surface increases with decreasing the indenter radius, finally reaching a value of 15 GPa. The same hardness value, 15 GPa, is also displayed by monocrystalline films indented to 2-nm depth with a sharp diamond indenter. In addition, scaling effect was demonstrated. The hardness decreases with increasing depth of indenter penetration, this being a result of the accumulation of stacking faults in the copper volume under the indenter. In the case in which a polycrystalline copper film with typical grain size 2 nm was indented with a spherical indenter no scaling effect in the dependences of estimated hardness on indenter radius and penetration was observed, with the hardness value being saturated at the level of 5-6 GPa.

This work was supported by the Russian Foundation for Basic Research (under Grant No. 11-01-00594-a) and by the Siberian Division of RAS (under integration programs).

References

[1] A. Gouldstone, H.-J. Koh, K.-Y. Zeng, A.E. Acta Mater. 48 (2000) 2277–2295.
[2] S. Suresh, T.-G. Nieh and B.W. Choi, Scripta Mater. 41(9) (1999) 951–957.
[3] L. Lu, R. Schwaiger, Z.W. Shan, M. Dao, K. Lu and S. Suresh, Acta Mater. 53 (2005) 2169 2179.
[4] A.V. Panin, A.R. Shugurov and K.V. Oskomov, Phys. Solid State 50(6) (2008) 2055.
[5] A.R. Shugurov, A.V. Panin and K.V. Oskomov, Phys. Solid State 50(6) (2008) 1050.
[6] Z. Huang, L.Y. Gu and J.R. Weertman, Scripta Mater. 37(7) (1997) 1071 1075.
[7] M.S. Daw, M.I. Baskes, Semiempirical, Phys Rev Lett 50 (1983) 1285 1288.
[8] M.S. Daw and M.I. Baskes, Phys Rev B 29 (1984) 6443 6453.
[9] A.V. Bolesta, I.F. Golovnev and V.M. Fomin, Phys. Mesomech. 3 (5) (2000) 37.
[10] A.V. Bolesta, I.F. Golovnev and V.M. Fomin, Phys. Mesomech. 4 (1) (2001) 5.
[11] A.V. Bolesta, I.F. Golovnev and V.M. Fomin, Phys. Mesomech. 5 (3-4) (2002) 101.
[12] S.J. Plimpton, J. Comp. Phys. 117 (1995) 1 19.
[13] C.L. Kelchner, S.J. Plimpton and J.C. Hamilton, Phys. Rev. B. 58 (1998) 11085 11088.
[14] A.V. Bolesta, V.M. Fomin, Phys. Mesomech. 14 (3-4) (2011) 107.
[15] M.F. Barnsley et al., The Science of Fractal Images. Springer-Verlag, 1988. – 312 p.
[16] B.N.J. Persson, O. Albohr, U. Tartaglino, A.I. Volokitin and E. Tosatti, J. Phys.: Condens. Matter. 17 (2005) R1–R62.
[17] W.G. Hoover, Phys. Rev. A. 31 (1985) 1695 1697.
[18] R.W. Siegel, G.E. Fougere. Nanostruct. Mater. 6, 205 (1995).
[19] A.V. Bolesta, V.M. Fomin, Phys. Mesomech. 12 (3-4) (2009) 117.
[20] M.I. Baskes, Phys. Rev. B 46(5) (1992) 2727-2742.